Characterization and origin of large size dust particles produced in the Alcator C-Mod tokamak

Cécile Arnas, James Irby, Sébastien Celli, Gregory de Temmerman, Younes Addab, Lenaic Couëdel, Christian Grisolia, Yijun Lin, Céline Martin, Cédric Pardanaud, et al.

Nuclear Materials and Energy 000 (2017) 1–8

Contents lists available at ScienceDirect

Nuclear Materials and Energy

journal homepage: www.elsevier.com/locate/nme

Characterization and origin of large size dust particles produced in the Alcator C-Mod tokamak

C. Arnas[a,*], J. Irby[b], S. Celli[a], G. De Temmerman[c], Y. Addab[a], L. Couëdel[a], C. Grisolia[d], Y. Lin[b], C. Martin[a], C. Pardanaud[a], S. Pierson[b]

[a] CNRS, Aix-Marseille université, Laboratoire PIIM, campus St Jérôme, 13397 Marseille, France
[b] M.I.T. Plasma Science and Fusion Center, 175 Albany Street, Cambridge, MA 02139, USA
[c] ITER Organization, Route de Vinon-sur-Verdon, 13067 St Paul Lez Durance, France
[d] IRFM/CEA Cadarache, 13108 St Paul Lez Durance, France

ARTICLE INFO

Article history:
Received 17 January 2017
Revised 22 February 2017
Accepted 23 February 2017
Available online xxx

Keywords:
Dust formation
Molybdenum
Tungsten
Boron
Alloy

ABSTRACT

Post mortem analyses of dust collected in Alcator C-Mod have highlighted a production of large size dust particles. The quantities of such large particles are higher than in any other tokamak. They are divided in two classes as a function of their shape and consequently, their origin. Rounded dust particles such as spheres and splashes constitute the first class. These particles are the result of high heat loads on various leading edges of plasma facing components and possibly, their melting during plasma operation. The heated or already molten material can be destabilized during disruptions and droplets are emitted across the vacuum chamber. After solidification, the resulting rounded particles are either in pure elements or in alloys. Flake-like dust particles, which are mainly due to light material coating delamination, constitute the second class of dust particles.

1. Introduction

Although the presence of dust in current tokamaks is not considered a safety issue, the French nuclear safety authority has imposed a limit on the dust inventory in ITER to avoid a possible dissemination during a LOVA (Loss Of Vacuum Accident) and a ICE (Ingress of Coolant Event). The possibility of dust mobilization during these potential accidents depends on the produced quantity and the adhesion forces, which maintain them on PFCs. In addition to safety issues, the mobilization of tungsten dust (ITER will use a full-W divertor) could be a source of high-Z contamination of the core plasma. These potential harmful situations have motivated many studies on dust production in tokamaks with graphite and metal PFCs: origins [1–6], characterization by post-mortem analyses [7–9], adhesion forces [10–12], transport [13–18], removal techniques [19,20] and influence on the performance of fusion devices [21–23]. However, among the wide variety of dust particles generated by plasma-wall interaction, none of the post-mortem investigations allowed a clear identification of those produced during instabilities (ELMs) and off-normal events such as VDEs or disruptions. Only fast cameras allowed a direct visualization of dust particles with size larger than 5–10 μm [24,25]. The lack of precise measurements in such conditions leads to large uncertainties on the size and kind of dust particles produced during off normal events in current tokamaks. These uncertainties make extrapolations difficult for ITER [26].

Post-mortem analyses presented in this paper allowed studying the shapes, compositions and sizes of dust particles generated in the full-metal tokamak, Alcator C-Mod. Elemental compositions established by energy dispersive X-ray spectroscopy (EDS) allowed selecting molybdenum (Mo), boron (B), tungsten (W) and the corresponding mixed material particles, which were produced by plasma-wall interaction. Size distributions established by scanning electron microscopy (SEM) revealed unexpected large average sizes (tens of μm), larger than those already established in other tokamaks with graphite and metal PFCs [2–5]. Two general dust shapes were identified, defining two different origins. Spherical and splash-like particles in pure Mo, W and B were found as well as in Mo-B and Mo-W alloys. Camera videos have shown that their origin is due to an overheating of various PFC leading edges during plasma operations -possibly their melting- followed by an emission of molten material droplets during disruptions [27,28]. B flake-like dust particles produced by the delamination of B layers

* Corresponding author.
E-mail address: cecile.arnas@univ-amu.fr (C. Arnas).

http://dx.doi.org/10.1016/j.nme.2017.02.027

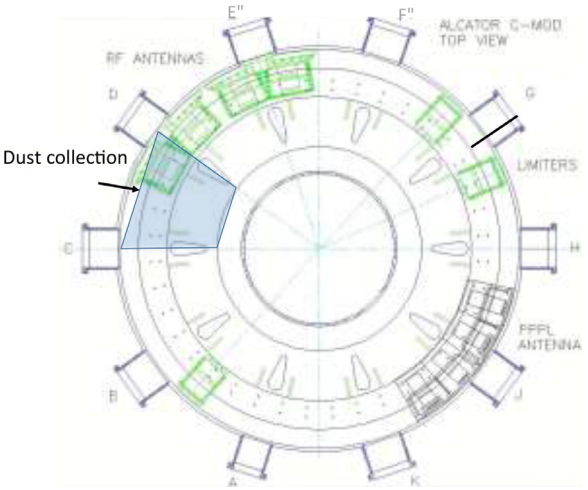

Fig. 1. Schematic of the Alcator C-Mod horizontal mid-plane showing 10 toroidal sectors corresponding to 10 lower outer divertor modules. Sectors are identified by the names: AB, BC... JK, KA. On the left side, the blue part shows where dust was collected in a given sector. (For interpretation of the references to color in this figure legend, the reader is referred to the web version of this article.)

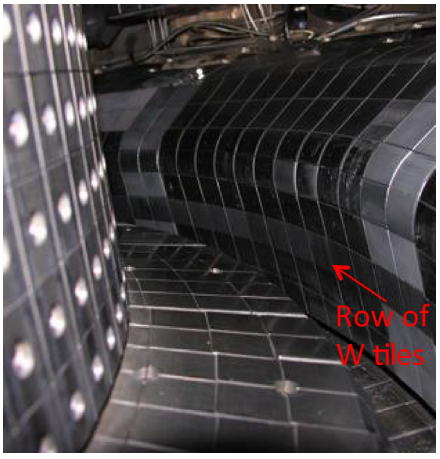

Fig. 2. View of the outer divertor, on the right side. A toroidal row of W tiles was inserted in 2007 in the strike point region and removed in 2010. An arrow indicates the W tile row position.

or B multi-layers were also identified and constitute the second class of particles in Alcator C-Mod.

2. Methods to select dust produced by plasma-wall interaction

Alcator C-Mod is a molybdenum–tokamak of 0.68 m major radius and 0.22 m minor radius, operating with a toroidal magnetic field of 3–8 T and a plasma current of 0.4–2 MA. It is divided in 10 toroidal sectors corresponding to 10 lower outer divertor modules. The sectors are identified by the names: AB, BC... JK, KA as shown in the schematic of Alcator C-Mod horizontal section (Fig. 1).

A toroidal row of W tiles was inserted in 2007 (Fig. 2), in the strike point region of the outer divertor and removed in 2010. Before the 2015 plasma campaign, the 10 outer divertor modules were slightly rotated by 1° to avoid damages on Mo tile edges.

Dust particles were collected at the end of 2007 and 2015 campaigns to identify differences. They were collected in almost all the sectors, using a vacuum cleaner (Atrix, model VACEXP-04E) loaded with HEPA filters of efficiency greater than 0.3 µm. For each investigated sector (~1 m^2), the vacuumed areas were the outer divertor module surface (~0.25 m^2), the floor between the outer and inner divertors, the area behind the outer divertor module when this PFC was removed and any other horizontal areas moving out toward the wall, including ports. For each plasma campaign, around 10 HEPA filters were used and identified by the name of the corresponding sector (AB, BC... JK, KA). Then, dust samples were transferred in glass boxes for characterization.

For a given sector, sieves of 500, 400, 300, 200, 100 and 50 µm openings were used to separate dust in samples of decreasing sizes. Sieves of 400/500 µm openings have eliminated the biggest pieces and debris coming from limiters, antennas and diagnostic environments (pieces of cables, insulators, welding, screws...) installed along the wall as well as dust coming from outside the vacuum chamber. EDS analyses were systematically done in parallel to SEM to identify Mo, B and W elements directly on samples. Another method consisted in transferring dust particles on the surface of fresh resin. After solidification, this resin was sanded and polished to obtain cross-sections of dust particles allowing the study of their internal composition.

Several samples were particularly contaminated with glass fibers, silver, ceramics, stainless steel debris and mica sheets with a broad size range. In a first study, only the least polluted samples coming from DE and EF sectors (RF antenna sectors as shown Fig. 1) were considered.

Size distributions were established from SEM measurements with the Saisam–Microvision software. It provides known contours (sphere, ellipse and other) to easily characterize spherical and elongated particles. The contour of irregular shaped particles is hand-drawn. Then, the software provides the equivalent diameter of the smallest circle in which the projection of all the particle contours can be circumscribed.

3. Origin of dust collected in tokamaks with graphite and metal PFCs

Earlier post-mortem analyses of dust collected in current tokamaks have shown that their origin depends on PFC materials, graphite or metal. However, in collected dust samples there was so far no clear identification of dust produced during off normal events such as disruptions.

In tokamaks with graphite PFCs, the dust production is mainly related to PFC chemical and physical erosion. A part of the eroded material goes back to PFCs to form co-deposited layers. Their delamination or flaking produce dust particles usually called, “flakes” [2,29]. Aggregates of spherical nanoparticles were also found and have two possible origins [29,30]: i) they can be initiated by molecular ions growing in the coldest plasma regions through specific collisions of hydrocarbon or carbon radicals, ii) they can also be generated by condensation of oversaturated carbon vapour when large thermal loads on PFCs produce graphite sublimation [2].

Laboratory experiments on disruption simulations have produced another dust category [31]. It was shown that during thermal loads delivering a power density much larger than that of graphite sublimation, graphite brittle destruction occurs and produces dust of 10′s of µm. However, brittle destruction was not clearly identified in graphite tokamak [32,33] while evidences were found in samples coming from the Extrap reverse field pinch [33,34].

Post-mortem analyses allowed concluding that in graphite tokamaks, the layer flaking during normal operations is the principal dust source and size distributions are usually lognormal. The average size found from all the dust distributions was (2.8 ± 2.4) µm [2]. The presence of large isolated flake-like dust (100′s µm) was also mentioned [1,2].

Please cite this article as: C. Arnas et al., Characterization and origin of large size dust particles produced in the Alcator C-Mod tokamak, Nuclear Materials and Energy (2017), http://dx.doi.org/10.1016/j.nme.2017.02.027

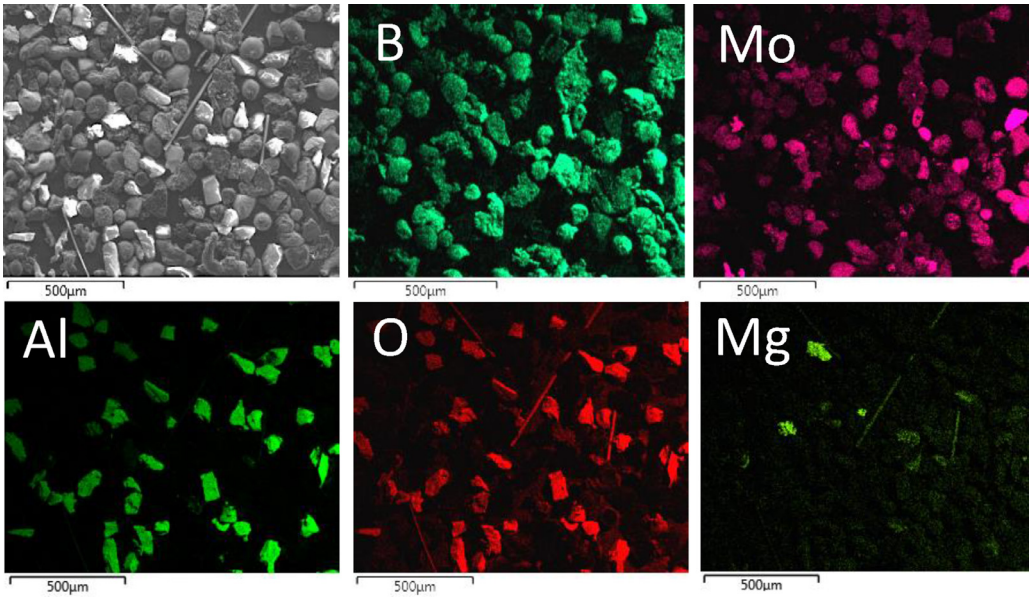

Fig. 3. SEM image of dust particles collected on DE sector (2015) with a size range of 50–100 µm. EDS mappings provide the sample composition: B, Mo, Al, O and Mg element positions are presented successively.

Regarding tokamaks with metal PFCs, analyses were performed to characterize dust samples, collected in comparable positions after several plasma campaigns in ASDEX Upgrade (AUG). Since AUG operates with W PFCs, no thick deposited layer was observed [3]. W-dominated particles were separated in two classes: spheres composed mainly of pure W or coated with light material and irregular-shaped particles. The latter were identified as conglomerates with varying W fraction in B-C matrices. Both classes were attributed to arcing on tile surfaces [35,36]. Their size distributions established over many plasma campaigns were fitted by lognormal functions. The sphere average size was ~2 µm and the irregular-shaped dust average size was ~1 µm [35]. The rare presence of large particles (10′s µm) was also mentioned and attributed to off normal events [3].

In the FTU tokamak equipped with a liquid lithium limiter (LLL), three dust categories were found [4]: spheroids, smashed droplets, both generated by melted material due to arcing and more likely to higher heat loads processes on PFCS, and flakes. Spheroids, consisting of almost exclusively Mo or stainless steel had diameters spanning from hundreds nm to µm. The final count median diameter was 1.87 µm and the geometric standard deviation was 2.09 µm. On the other hand, lithium-based dusts, with sizes extending up to a few mm were also found inside the duct where the LLL is installed.

In JET-ILW, after the first shutdown, a tiny number of dust particles was analysed. These particles were found on the apron of the so-called tile 1, located in the inner divertor [5]. Analytical studies were performed for instance on a Be flake with 50×70 µm size, a 5 µm Be droplet and a ~20 µm W-based agglomerate originating from W coating on carbon tiles. Interestingly, empty W spheroids with ~5µm sizes were also collected.

Dedicated melt experiments of W surfaces were carried-out in TEXTOR by using the movable sample manipulator, which was introduced inside the LCFS [37]. Melt layer motion and ejection of dust into the plasma were studied using a 2D camera system. A spray of fine particles (µm range) was observed together with some random large droplets looking as splashes (10–100 µm). Post mortem analyses of redeposited droplets provided an average size of 4 µm. Some particles with a 10–20 µm size range were also found while largest droplets were found as single occurrences and the smallest ones (spray) were difficult to find.

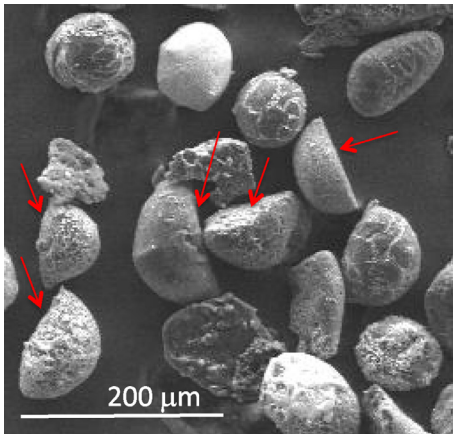

Fig. 4. Rounded-shape dust with a size range of 100–200 µm, collected in EF sector (2007). Arrows show hemispheres. Flat faces indicate a contact with PFC surfaces.

4. Compositions and morphologies of dust collected in Alcator C-Mod DE-EF sectors

4.1. Direct analyses of dust samples with SEM and EDS

SEM image of Fig. 3 shows dust particles with a size range of 50–100 µm (DE sector-2015). EDS mappings give the spatial distribution of dominant elements: B, Mo, Al, O and Mg. The B and Mo mapping subtraction indicates in a first approach that not all of Mo particles have a B-coating due to wall boronization and that pure B dust also exists. This result will be developed further in the text. The presence of Al and O indicates the presence of ceramic debris most likely coming from alumina insulators (Al_2O_3) on divertor components. Glass fibers (Si, O, Mg, Ca, Na, K) most likely coming from the insulation used around instrumentation cables are also present but only O and Mg elements of their composition are shown. Isolated Mg-dominated dust also appears. Cu and steel (Fe, Ni, Cr, Mo) isolated dusts were also identified but not shown. The fraction of contaminant dust was 28%. Generally, traces of all materials coming from the equipment installed in the vacuum chamber appear in EDS spectra but only elements showing sufficient high X-ray lines were considered.

Please cite this article as: C. Arnas et al., Characterization and origin of large size dust particles produced in the Alcator C-Mod tokamak, Nuclear Materials and Energy (2017), http://dx.doi.org/10.1016/j.nme.2017.02.027

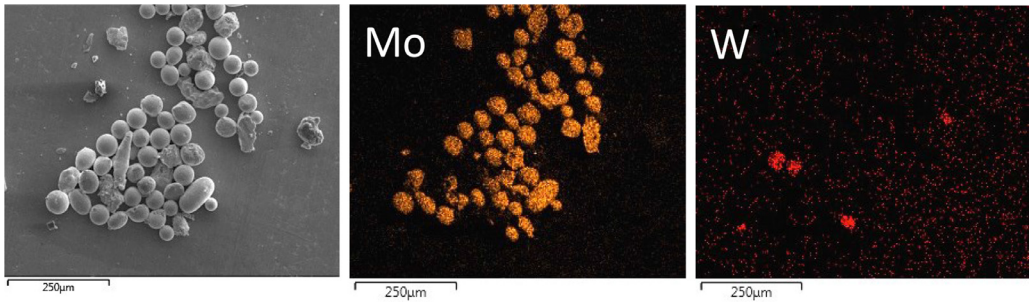

Fig. 5. Dust particles with 42 µm average size (DE sector-2007) mainly composed with Mo spheres and some W spheres. Steel spheres and irregular Ag dusts were also identified but not shown by EDS.

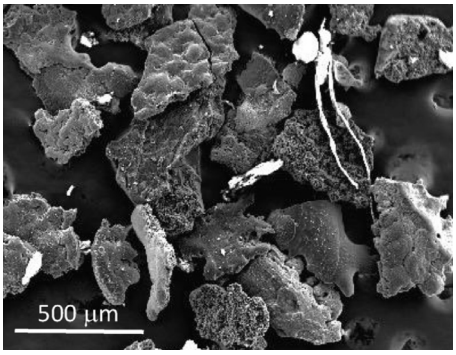

Fig. 6. Sample mainly composed of B-flakes with a size range of 200–300 µm (DE sector-2015).

Fig. 4 shows an example of rounded-shape particles (EF sector-2007) with a size range of 100–200 µm. Some of them have spheroid shapes, other are half-spheres. The flat faces (red arrows) indicate a contact with PFC surfaces. Although compositions are established with EDS, it should be noted that under the SEM electron beam, the higher the atomic number of an element, the brighter it appears. Thus, the white particle at the top of the image consists mainly of Mo while neighboring spheres (left and right of the white sphere) consist of B and Mo mixture (dark and white, respectively) as well as the two half-spheres at the bottom left side and the two quasi-spheres at the bottom right side. The dark elongated particle at the top right side is made of B-dominated material.

Fig. 5 shows dust particles with a size range of 0–50 µm coming from the DE sector-2007. Around 50% of all the particles collected in this sector with a 50 µm sieve opening are spheres of 42 µm average size. In the sample showed in Fig. 5, 73% of particles are spheres. 80% of these spheres are in Mo, 8.5% in W, 8.5% in steel (not shown in Fig. 5) and 3% in Ag (not shown in Fig. 5).

Fig. 6 shows a second dust category. They mainly consist in flat pieces of B coatings, looking like flakes with a size range of 200–300 µm (DE sector-2015). One of them at the top of the image is broken. At the bottom, another one of ~30 µm thickness is almost perpendicular to the substrate. Pieces of glass fibers appear oversaturated since they cannot conduct correctly the charges from the microscope electron beam.

4.2. Dust cross-section analyses by SEM and EDS

Since EDS mapping cannot give elemental compositions along thickness deeper than 10′s µm, dust cross-sections were also analyzed (preparation described in Chap. 2). Fig 7 shows the cross-sections of a ~300 µm Mo particle (DE sector-2007), a ~180 µm B sphere (DE sector-2007) and a ~120 µm W sphere (EF sector-2007), with the respective compositions given by EDS spot-mode spectra. This investigation has confirmed the production of pure B, Mo and W rounded particles with sizes larger than 100 µm.

Fig. 8-a) shows the cross-section of a rounded dust of B-Mo mixed material (DE sector-2007). One can roughly deduce information on this alloy formation from the material structure. Fig. 8-b) shows the existence of a heterogeneous binary alloy with a limited solubility of B and Mo. It is composed of large B grains (dark grains) and a structured B-Mo mixture. Alternate bright and dark layers (lamellar microstructure) in various areas are characteristic of eutectic mixture. At the eutectic point, as for a pure element, the liquid transforms simultaneously in two solid phases at a unique temperature (eutectic temperature), lower than the melting temperature of each component. Let us recall that the Mo and B melting temperatures are 2623 °C and 2075 °C, respectively. The presence of large B grains indicates that in the initial mixture, B was dominant and started the solidification at 2075 °C. This resulted in the presence of growing B grains in a B-Mo melted mixture during the cooling from the B melting temperature to the lower eutectic temperature. In other words, the solidification of B grains continued until enough Mo atoms were removed so that the remaining liquid was of eutectic composition and the solidification of the resulting mixture appeared at the eutectic temperature. Generally, all the analyzed B-Mo dust particles present a similar microstructure.

Fig. 9-a) shows the cross-section of a particle, which consists of W (white) and B (dark) grains (EF sector-2007). The microstructure highlighted in the zoomed image (Fig. 9-b) shows a heterogeneous binary alloy with a limited solubility of B and W. The grain sizes and arrangements vary greatly into the dust. In particular, W and B grain sizes in the left part of Fig. 9-b) are larger than in the right part. No obvious organized microstructure, characteristic of a eutectic composition was observed in this dust. Unfortunately, only a few such particles were found so that a more detailed characterization was not possible.

5. Size distributions

Using EDS, size distributions were only established with dust in Mo, B and Mo-B alloy. Fig. 10-a) gives the size distribution of dust coming from 2007-DE and 2007-EF sectors. For each sector, size measurements were performed on samples obtained with successive sieve openings. Then, the obtained histograms were added to provide the final size distribution. The sizes of 1697 particles, which constitute just a part of the dust quantity produced in these sectors, were measured in this way. Fig. 10-b) gives the size distribution of a dust particle part coming from the 2015-DE sector (1065 particles). In this case, the sizes of all particles sieved with a 50 µm opening, were measured. With a bin width of 20 µm, in both cases, the most probable size is ~50 µm and the maximum size is ~450 µm. In both cases, the largest sizes are mostly provided

Please cite this article as: C. Arnas et al., Characterization and origin of large size dust particles produced in the Alcator C-Mod tokamak, Nuclear Materials and Energy (2017), http://dx.doi.org/10.1016/j.nme.2017.02.027

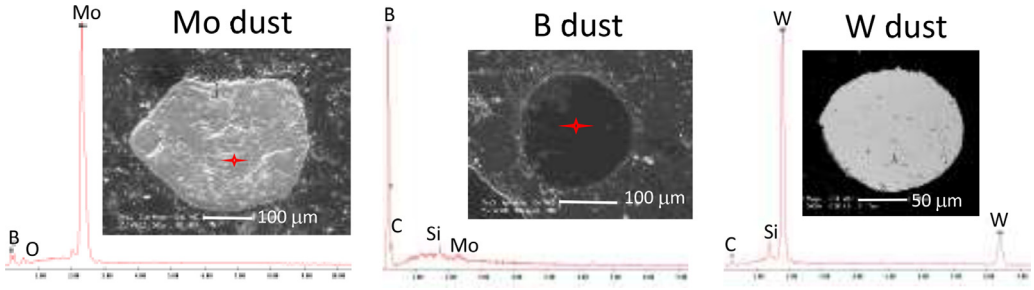

Fig. 7. Cross-sections of a ~300 µm Mo dust (DE sector-2007), a ~180 µm B sphere (DE sector-2007) and a ~120 µm W sphere (EF sector-2007). EDS spot-mode spectra give the respective compositions.

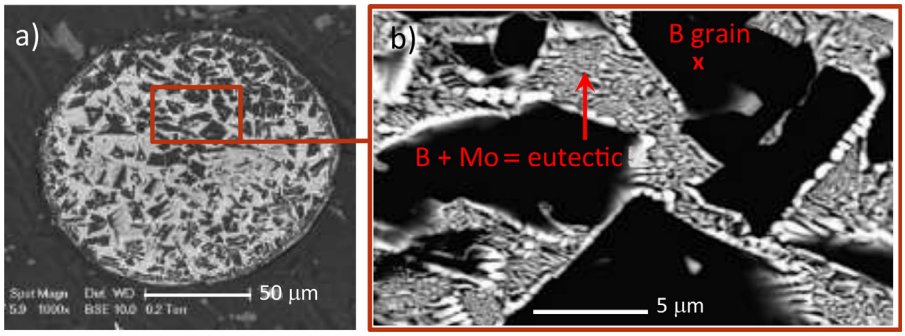

Fig. 8. a) Cross-section of a ~125 µm dust in B-Mo alloy; b) magnification showing two solid phases: B grains (dark) are mixed with a B-Mo mixture of lamellar microstructure, characteristic of an eutectic composition.

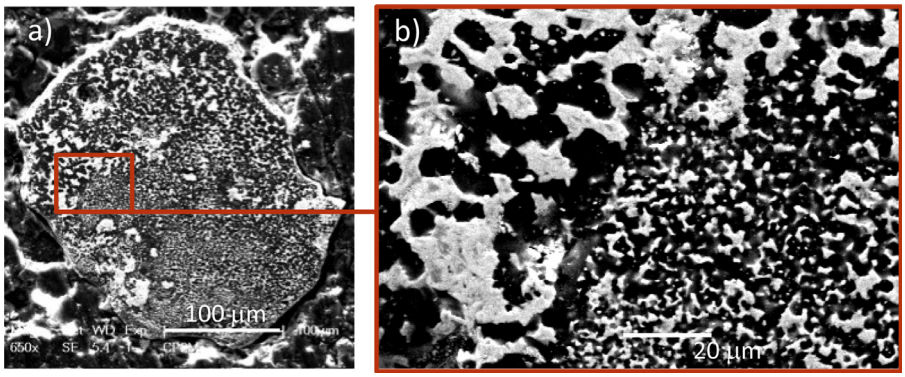

Fig. 9. a) Cross-section of a ~255 µm dust in W-B alloy; b) magnification of a heterogeneous solid. The B-dominated phase (dark) and W-dominated phase (white) have different proportions on the left and right parts of the image.

by thin splash-like and thin flake-like particles while the smallest ones are mostly round thick particles. In the final size histogram, 80% (84%) of the 2007 (2015) particles contain Mo, i.e. pure Mo and Mo-B alloy, the remaining dust being made of pure B.

It is important to add that smaller dust particles than those presented in the distributions of Fig. 10 exist very probably. The main property of HEPA filters being to trap dust particles inside a mat of randomly arranged fibres, no information can be obtained on these small sizes.

6. Discussion on the dust origin in alcator C-Mod

The video snapshots (visible camera) of Fig. 11 show a typical example of a molten material droplet emission after a major disruption going upward during the 2016 plasma campaign. The disruption occurred between the snapshots of Fig. 11-a) and Fig. 11-b). After the disruption (Fig 11-b) and c)), droplets of molten material were ejected from radial tile edges, which were glowing during the plasma phase, before the disruption (top of Fig 11-a)- arrow showing an example). The majority of these droplets were transported in the vacuum chamber around the central column from the left to the right side. The plasma began with a lower single null diverted that was moved to an upper single null diverted. ICRF heating (3.5 MW) was turned on during the later configuration.

Fig. 12-a) shows a part of the upper divertor (left side) and the radial slots (center part) leading to the cryopumps [38]. The addition of ICRF heating leads to an over-heating of these slots edges, which can begin to melt (Fig. 11-a)). Some videos indeed show that some molten material droplets can already be expelled from these glowing regions during plasma operation. After disruptions going upward, the tile edges from which droplets are emitted still remain glowing for some time as shown by arrows in Fig 11-c). Fig. 12-b) shows an example of the resulting damage. Mo melting appears on the parts of the tile leading edge and surface, which are in contact with the upper divertor target (left part of the image). Three long irregular, redeposited melts are also present on the tile surface (central square of Fig. 12-b)).

Fig. 13 shows melt damage on a sector leading edge of the outer divertor. The initial misalignment of this sector is at the origin of the melting of the tile edges receiving high parallel heat

Please cite this article as: C. Arnas et al., Characterization and origin of large size dust particles produced in the Alcator C-Mod tokamak, Nuclear Materials and Energy (2017), http://dx.doi.org/10.1016/j.nme.2017.02.027

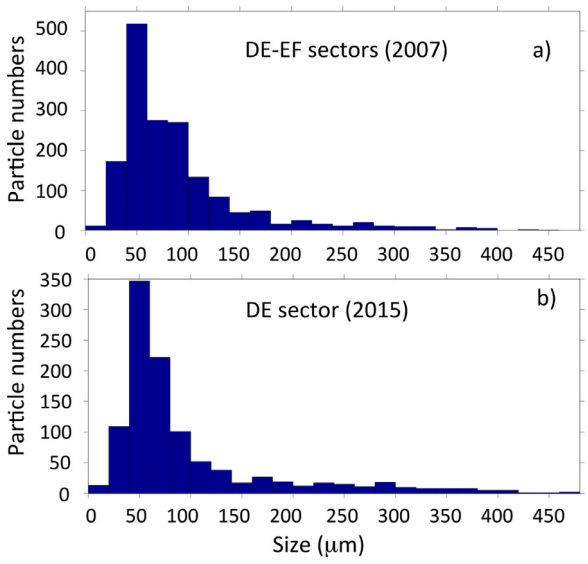

Fig. 10. a) Size distribution of 1697 particles coming from 2007-DE and 2007-EF sectors; b) size distribution of 1065 particles coming from 2015-DE sector. In both cases, the most probable size is ~50 μm and the maximum is ~450 μm.

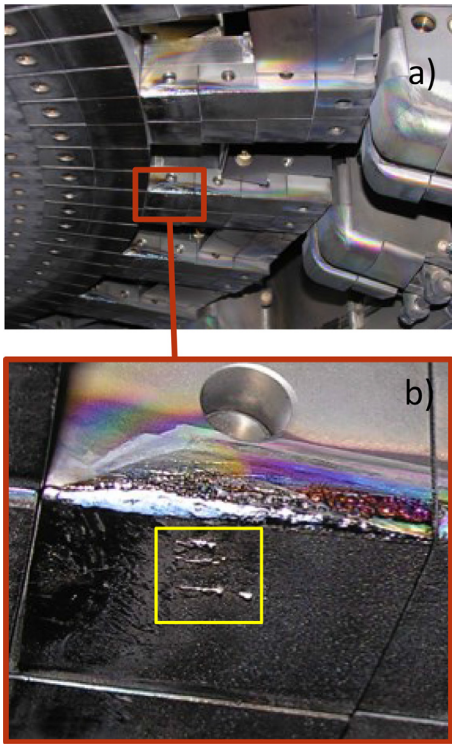

Fig. 12. a) Part of the upper divertor (left side) and radial slots (center part) leading to the neutral cryopumps. Damages on the slot tiles are produced radially. Whitish and colored coatings on components, which are far from the strike point region result from many boronization sequences; b) magnification showing that Mo melting takes place on the tile surfaces and leading edges, which are in contact with the upper divertor target. Three long Mo redeposited melts are present on the tile surface (into the central square).

fluxes in the strike point region (C-Mod has a high parallel heat flux owing to its high magnetic field and small size) [39]. To suppress melting damage, instead of toroidaly aligning the divertor sectors, a slight rotation around the middle of each sector was performed at the beginning of the 2015 campaign. The goal was to shadow each module leading edge by the upstream neighboring sector. As expected, a visual inspection after the chamber venting assured that few damage were produced during the plasma campaign even though disruptions going downward and upward were still produced. Moreover, the quantity of dust transferred from all the HEPA filter cartridges (a filter for almost each sector) towards boxes for sampling was smaller in 2015 than in 2007. Several mass measurements were then performed and have provided rough estimations of the produced quantities. In particular, it is impossible to estimate the dust quantity, which can be trapped in HEPA filters; there was a high adherence of smallest dust particles on the walls of canisters and on several plastic boxes where they were transferred for further sampling; there was a general contamination of B, Mo and W dust particles by dust-debris of various composition and in the sieve samples of dust coming from DE-, EF-2007 and DE-2015 sectors, contaminant dust appeared with various percentages. Within these limits, the mass of dust particles coming from EF-2007 sector and transferred from HEPA filter canisters (~194.5 mg) was on average ~3 times larger than the mass of dust transferred from the EF-2015 filter canister; the ratio of the transferred dust masses was ~4 in the case of DE sector (2007/2015) and ~6 in the case of FG sector (~430 mg was transferred from the FG-2007 filter canister). These results, added to the fact that the average energy injected in 2280 discharges in 2015 was 0.66 MJ/discharge against 2026 discharges in 2007 with 0.45 MJ/discharge, may indicate that less dust was produced in 2015. These results also suggest that the dust production was not toroidally homogeneous.

Regarding W dust, less than 25 particles were found in the samples of DE-EF sectors (2007). Their rounded shapes (spheres, splashes-like) associated with large sizes (40–150 μm) indicate that they were produced during severe heat loads on the W tile row

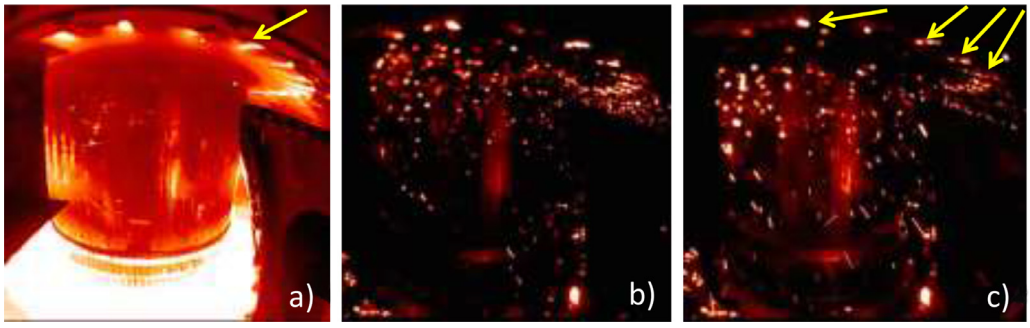

Fig. 11. a) Video snapshot showing the glowing of radial tile edges, located in the upper divertor region as well as the glowing of the surrounding plasma (1.35 s). These light emissions appear during ICRF heating. The image was taken just before a disruption going upward (1.47 s); b) and c), after disruption (1.52 s, 1.54 s respectively), droplets of molten material are ejected from the tile edges, which were glowing before disruption. Droplets that appear as hot spots around the central column are transported from the left to the right side in the vacuum chamber (image coordinate).

Please cite this article as: C. Arnas et al., Characterization and origin of large size dust particles produced in the Alcator C-Mod tokamak, Nuclear Materials and Energy (2017), http://dx.doi.org/10.1016/j.nme.2017.02.027

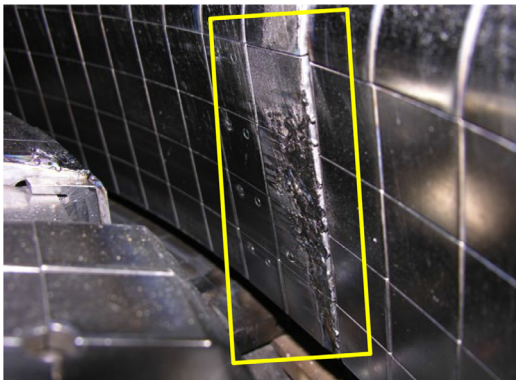

Fig. 13. Detail of the leading edge of an outer divertor module. The tiles of the leading edge were melted repeatedly during the 2007 plasma campaign due to their misalignment.

that was toroidaly inserted in the outer divertor strike point region (no available image of W damage during the 2007 campaign). The low number of W particles could suggest that they were produced from other sectors and then transported towards DE-EF sectors. Note that even if the W melting temperature (3425 °C) is larger than the one of Mo, W and Mo dust sizes are in the same size range

Fig. 12-a) also shows the presence of a whitish coating (right side of the image) on component surfaces far from the strike point region, resulting from frequent boronization sequences [40]. The presence of colored layers in other locations could be due to light interferences or heating variations on thin coatings. Conversely, the presence of B flake-like particles is explained by the delamination of badly adherent thicker layers or multilayers. Rounded edges of a large part of them also suggest delamination under high heat loads.

7. Conclusion

Post-mortem analyses of dust collected in Alcator C-Mod after the 2007 campaign (installation of a toroidal row of W tiles in the outer divertor and removed in 2010) and the 2015 campaign (slight rotation of the outer divertor modules) have highlighted a production of large size dust, in higher quantities than in any other tokamak. Size distributions show that for both plasma campaigns, the most probable size is ~50 µm and the largest sizes can reach 450 µm. B flake-like dusts, which mainly compose the largest particles, come from the delamination of B layers or multilayers. Rounded dust particles such as spheres and splash-like particles in pure Mo, B, W and in mixed materials are coming from an emission of the corresponding molten materials. Camera videos of plasma operations as well as visual inspections of the PFCs after plasma campaigns allowed finding their origins. The slot edges of the cryopumps and the leading edges of the 10 outer divertor modules when these later are misaligned are overheated and can melt during plasma operations. Large size droplets of molten material are then emitted repeatedly from these regions during disruptions, in addition to some droplets, which could be emitted during the plasma. A slight rotation of all the outer divertor modules was performed in 2015, in order to shadow their leading edges by the upstream neighboring sector. As expected, much less damages were observed at the end of the plasma campaign and less dust particles were collected although disruptions going downward and upward were still produced.

Acknowledgments

Authors wish to thank G. Giacometti from Aix-Marseille université/laboratoire PIIM for his technical assistance during the dust cross-section procedure and M. Cabié from Aix-Marseille Université/CP2M for her advises on SEM. This work was supported by a grant coming from the French Fédération de Recherche Fusion par Confinement Magnétique. The views and opinions expressed herein do not necessarily reflect those of the ITER Organization.

References

[1] J. Winter, G. Gebauer, J. Nucl. Mater. 266-269 (1999) 228.
[2] J.P. Sharpe, D.A Petti, H.-W. Bartels, Fusion Eng. and Design 63-64 (2002) 153.
[3] V. Rohde, M. Balden, T. Lunt the ASDEX Upgrade team, Phys. Script. T138 (2009) 014024N.
[4] M. De Angelis, G. Maddaluno, L. Laguardia, D. Ripamonti, E. Perelli Cippo, M.L. Apicella, C. Conti, G. Giacomi, G. Grosso, J. Nucl. Mater. 463 (2015) 847.
[5] A. Baron-Wiechec, E. Fortuna-Zalesna, J. Grzonka, M. Rubel, A. Widdowson, C. Ayres, J.P. Coad, C. Hardie, K. Heinola, G.F. Matthews JET Contributers, Nucl. Fusion 55 (2015) 113033.
[6] C. Grisolia, S. Rosanvallon, A. Loarte, P. Sharpe, C. Arnas, J. Nucl. Mater. 390-391 (2009) 53.
[7] M. Richou, C. Martin, P. Delhaès, M. Couzi, W. Saikaly, C. Brosset, B. Pégourié, A. Litnovsky, V. Philipps, P. Wienhold, J. Dentzer, C. Vix-Guterl, P. Roubin, Carbon 45 (2007) 2723.
[8] C. Arnas, C. Pardanaud, C. Martin, P. Roubin, G. De Temmerman, G. Council, J. Nucl. Mater. 401 (2010) 130.
[9] E. Fortuna-Zalesna, J. Grzonka, M. Rasinski, ., M. Balden, V. Rohde, K.J. Kurzydlowski the ASDEX Upgrade team, Phys. Scr. T159 (2014) 014066.
[10] L. Begrambekov, A. Grunin, A. Zakharov, Nucl. Instrum. and Methods Plasma Phys. B 354 (2015) 282.
[11] S. Ratynskaia, P. Tolias, I. Bykov, D. Rudakov, M. De Angeli, L. Vignitchouk, D. Ripamonti, G. Riva, S. Bardin, H. van der Meiden, Nucl. Fusion 56 (2016) 066010.
[12] A. Rondeau, J. Merrison, J.J. Iverson, S. Peillon, J.C. Sabroux, P. Lemaitre, F. Gensdarmes, E. Chassefiere, Fusion Eng. Design 98-99 (2015) 2210.
[13] A. Yu Pigarov, S.I. Krasheninnikov, T.K. Soboleva, T.D. Rognlien, Phys. Plasma 12 (2005) 122508.
[14] D.L. Rudakov, W.P. West, C.P.C. Wong, N.H. Brooks, T.E. Evans, M.E. Fenstermacher, M. Groth, S. Krasheninnikov, C.J. Lasnier, et al., J. Nucl. Mater. 363-365 (2007) 227.
[15] Suk-Ho Hong, C. Grisolia, V. Rohde, P. Monier-Garbet ASDEX Upgrade Team, Nucl. Fusion 50 (2010) 035002.
[16] G. De Temmerman, M. Bacharis, J. Dowling, S. Lisgo, Nucl. Fusion 50 (2010) 105012.
[17] S. Bardin, J-L. Briancon, F. Brochard, V. Martin, Y. Zayachuk, R. Hugon, J. Bougdira, Contrib. Plasma Phys. 51 (2011) 246.
[18] A. Shalpegin, F. Brochard, S. Ratynskaia, P. Tolias, M. De Angeli, L. Vignitchouk, I. Bykov, S. Bardin, K. Bykov, T. Morgan, G. De Temmerman, Nucl. Fusion 55 (2015) 112001.
[19] A. Vatry, A. Marchand, Ph. Delaporte, C. Grisolia, C. Hernandez, H. Roche, M. Sentis, J. Nucl. Mater. 415 (2011) S1115.
[20] S. Paci, M.T. Porfiri, Fusion Eng. and Design 83 (2008) 151.
[21] A. Ekedahl, J. Bucalossi, Y. Corre, E. Delchambre, G. Dunand, O. Meyer, R. Mitteau, P. Monier, et al., J. Nucl. Mater. 390-391 (2009) 550.
[22] S.I. Krasheninnikov, R.D. Smirnov, D.L. Rudakov, Plasma Phys. Control. Fusion 53 (2011) 083001.
[23] A. Litnovsky, D.L. Rudakov, S. Bozhenkov, R.D. Smirnov, S. Ratynskaia, H. Bergsaker, I. Bykov, N. Ashikawa, G. De Temmerman, Y. Xu, et al., J. Nucl. Mater. 438 (2013) S126.
[24] D.L. Rudakov, A. Litnovsky, W.P. West, J.H. Yu, J.A. Boedo, B.D. Bray, S. Brezinsek, N.H. Brooks, M.E. Fenstermacher, et al., Nucl. Fusion 49 (2009) 085022.
[25] S-H. Hong, K-R Kim, Y-U Nam, J. Chung, C. Grisolia, V. Rohde ASDEX Upgrade team, Nucl. Instrum. Methods Phys. Research A 720 (2013) 105.
[26] M. Shimada, R.A. Pitts, S. Ciattaglia, S. Carpentier, C.H. Choi, G. Dell Orco, T. Hirai, A. Kukushkin, S. Ligo, J. Palmer, W. Shu, E. Veshchev, J. Nucl. Mater. 438 (2013) S996.
[27] A. Hassanien, I. Konkashbaev, J. Nucl. Mater. 290-293 (2001) 1074.
[28] B. Bazylev, I. Landman, A. Loarte, N.S. Klimov, V.L. Podkovyrov, V.M. Safronov, Phys. Scr. T138 (2009) 014061.
[29] J. Winter, Plasma Phys. Control. Fusion 46 (2004) B583.
[30] C. Arnas, C. Martin, P. Roubin, B. Pégourié, G. De Temmerman, K. Hassouni, A. Michau, G. Lombardi, X. Bonnin, Plasma Phys. Control. Fusion 52 (2010) 124007.
[31] J. Linke, S. Amouroux, E. Berthe, Y. Koza, W. Kuhnlein, M. Rodig, Fusion Eng. Design 66-68 (2003) 395.
[32] D. Ivanovna, M. Rubel, V. Philipps, M. Freisinger, Z. Huang, H. Penkalla, B. Schweer, G. Sergienko, P. Sundelin, E. Wessel, Phys. Scr. T138 (2009) 014025.
[33] J. Linke, M. Rubel, J.A. Malmberg, J.R. Drake, R. Duwe, H.J. Penkalla, M. Rodig, E. Wessel, Phys. Script. T91 (2001) 36.
[34] M. Rubel, M. Cecconello, J.A. Malmberg, G. Sergienko, W. Biel, J.R. Drake, A. Hedqvist, A. Huber, V. Philipps, Nucl. Fusion 41 (2001) 1087.
[35] V Endstrasser, M. Rohde, P. Balden, U. Humrickhouse, B.J. von Toussaint, H-K. Braams, R. Chung Neu and the ASDEX Upgrade team, Phys. Scr. T45 (2011) 014021.
[36] M. Balden, N. Endstrasser, P. Humrickhouse, V. Rohde, M. Rasinski, U. von Toussaint, S. Elgeti, R. Neu The ASDEX Upgrade team, Nucl. Fusion 54 (2014) 073010.

Please cite this article as: C. Arnas et al., Characterization and origin of large size dust particles produced in the Alcator C-Mod tokamak, Nuclear Materials and Energy (2017), http://dx.doi.org/10.1016/j.nme.2017.02.027

[37] J.W. Coenen, B. Bazylev, S. Brezinsek, V. Philipps, T. Hirai, A. Kreter, J. Linke, G. Sergienko, A. Pospieszczyk, T. Tanabe, Y. Ueda, U. Samm the TEXTOR team, J. Nucl. Mater. 415 (2011) S78.
[38] J. Zaks, R. Viera, H. Savelli, B. LaBombard, J. Irby, P. Titus, R. Childs, A. Zhukovsky, in: 20TH IEEE/NPSS Symposium on Fusion Engineering, IEEE, NY 10017 USA, PROCEEDINGS, Publisher, 2003, p. 62, doi:10.1109/FUSION.2003.1425878.
[39] R.S. Granetz, I.H. Hutchinson, J. Sorci, J.H. Irby, B. LaBombard, D. Gwinn, Nucl. Fusion 36 (1996) 545.
[40] B. Lipschultz, Y. Lin, E.S. Marmar, D.G. Whyte, S. Wukitch, I.H. Hutchinson, J. Irby, B. LaBombard, M.L. Reinke, J.L. Terry, G. Wright The Alcator C-Mod Group, J. Nucl. Mater. 363-365 (2007) 1110.

Please cite this article as: C. Arnas et al., Characterization and origin of large size dust particles produced in the Alcator C-Mod tokamak, Nuclear Materials and Energy (2017), http://dx.doi.org/10.1016/j.nme.2017.02.027